

Tislelizumab uniquely binds to the CC' loop of PD-1 with slow-dissociated rate and complete PD-L1 blockage

Yuan Hong , Yingcai Feng, Hanzi Sun, Bo Zhang, Hongfu Wu, Qing Zhu, Yucheng Li, Tong Zhang, Yilu Zhang, Xinxin Cui, Zhuo Li, Xiaomin Song, Kang Li, Mike Liu and Ye Liu 

BeiGene Global Research, BeiGene (Beijing) Co., Ltd., China

Keywords

anti-PD-1 antibody; BGB-A317; epitope mapping; PD-1; tislelizumab

Correspondence

Y. Liu, BeiGene Global Research, BeiGene (Beijing) Co., Ltd., Beijing 102206, China
Tel: +86-010-58254385
E-mail: ye.liu@beigene.com

Yuan Hong and Yingcai Feng contributed equally to this work

(Received 6 September 2020, revised 18 December 2020, accepted 27 January 2021)

doi:10.1002/2211-5463.13102

Edited by Cláudio Soares

Programmed cell death protein 1 (PD-1), an immune checkpoint receptor expressed by activated T, B, and NK cells, is a well-known target for cancer immunotherapy. Tislelizumab (BGB-A317) is an anti-PD-1 antibody that has recently been approved for treatment of Hodgkin's lymphoma and urothelial carcinoma. Here, we show that tislelizumab displayed remarkable antitumor efficacy in a B16F10/GM-CSF mouse model. Structural biology and Surface plasmon resonance (SPR) analyses revealed unique epitopes of tislelizumab, and demonstrated that the CC' loop of PD-1, a region considered to be essential for binding to PD-1 ligand 1 (PD-L1) but not reported as targeted by other therapeutic antibodies, significantly contributes to the binding of tislelizumab. The binding surface of tislelizumab on PD-1 overlaps largely with that of the PD-L1. SPR analysis revealed the extremely slow dissociation rate of tislelizumab from PD-1. Both structural and functional analyses align with the observed ability of tislelizumab to completely block PD-1/PD-L1 interaction, broadening our understanding of the mechanism of action of anti-PD-1 antibodies.

Immune responses mediated by T cells are triggered when the antigenic peptide/HLA complexes on antigen-presenting cell (APC) surface are recognized by T-cell receptors (TCR). The regulation of these T-cell-mediated immune responses is balanced by antigen-independent costimulatory or coinhibitory coreceptor signals [1–3]. T cells can recognize the tumor-specific antigens presented on the surface of cancer cells, causing immune response against the cancer. However, cancer cells also develop some tumor-induced immune suppression mechanisms to evade immunological recognition [4,5]. One of the mechanisms of immune suppression is to upregulate the expression of immune suppressive molecules or their ligands or receptors, for example LAG-3, galectin-9/TIM-3, CTLA4, and programmed death-1 (PD-1), inhibiting the activation of effector T cells, thus

leading to poor response by the immune system to the cancer [6].

As a well-known immune checkpoint molecule, PD-1 is expressed in multiple types of immune cells, including activated T cells, B cells, certain dendritic cells (DCs), natural killer (NK) cells, and monocytes [7]. When binding to its natural ligands, PD-1 ligand 1 (PD-L1) or PD-1 ligand 2 (PD-L2), PD-1 activates intracellular signaling pathways and inhibits the activation of immune cells [8,9]. Previous studies have shown that immune suppression occurs in the tumor microenvironment while upregulating expression of PD-1 and PD-L1 in T cells and tumor cells, respectively [4,5]. Thus, blocking the PD-1 pathway has become a key direction to abolish immune suppression for immunotherapy, and the development of

Abbreviations

i.p., intraperitoneal; RU, responsive unit; SPR, surface plasmon resonance; TGI, tumor growth inhibition; V_H, variable region of heavy chain; V_L, variable region of light chain.

monoclonal antibodies targeting PD-1 or PD-L1 has been a research ‘hot spot’ of tumor immunotherapy in recent years [10–15]. Two antibodies targeting PD-1, pembrolizumab (Merck & Co., Inc., Kenilworth, NJ, USA) and nivolumab (Bristol-Myers Squibb, New York, NY, USA), have been approved for treatment of bladder cancer, renal cell carcinoma, melanoma, Hodgkin’s lymphoma, non-small-cell lung cancer, and other tumors by the US Food and Drug Administration (FDA) since 2014 [16]. Tislelizumab (BGB-A317), an anti-PD-1 antibody, has been approved recently as a treatment for patients with classical Hodgkin’s lymphoma who have failed at least one prior therapy or patients with locally advanced or metastatic urothelial carcinoma. Additionally, tislelizumab is being evaluated in global pivotal trials in a wide range of tumors, including esophageal squamous cell carcinoma, hepatocellular carcinoma, and non-small-cell lung cancer [17].

Previous structural biology studies on the complexes of PD-1 with pembrolizumab or nivolumab have provided valuable information for understanding the binding mechanism of these two approved anti-PD-1 therapies [18–20]. In this study, we investigated the anti-tumor efficacy of tislelizumab and its binding kinetics to PD-1, and then identified the key epitopes of tislelizumab by both structural biology study and surface plasmon resonance (SPR) analysis. Both the structural and functional studies revealed the unique interaction of tislelizumab with PD-1 and provided insight into its mechanism of action by completely blocking the interaction of PD-1 with PD-L1. This work represents the first report to demonstrate the CC’ loop of PD-1 as a targetable region for anti-PD-1 antibodies.

Materials and methods

Key materials

The hPD-1 C57BL/6 transgenic mice used for *in vivo* efficacy evaluation were purchased from Biocytogen Co., Ltd. (Beijing, China). The antibodies pembrolizumab and nivolumab were purchased from Selleckchem (Houston, TX, USA), while tislelizumab was a gift from BI (Shanghai, China). HEK293F cells expressing recombinant PD-1 or tislelizumab Fab proteins were obtained from Thermo Fisher (Shanghai, China).

In vivo efficacy study

B16F10/GM-CSF tumor cells (5×10^4) were implanted subcutaneously in hPD-1 C57BL/6 transgenic mice. On the day of implantation, mice were randomized into two

groups and then treated with PBS (vehicle) or 10 mg·kg⁻¹ of tislelizumab intraperitoneally (i.p.) once a week for 4 weeks. Tumor volume was measured twice weekly. All experiments involving animals were conducted based on the protocols approved by the Animal Care and Use Committee of BeiGene according to the guidelines of the Chinese Association for Laboratory Animal Sciences.

Plasmid construction and site-directed mutagenesis

The coding sequences of heavy and light chains of tislelizumab Fab were cloned into pMax vector, respectively, with a hexa-His tag at the C terminus of heavy chain for purification. The DNA encoding the ectodomain of hPD-1 (residues M1-T170, including signal peptide, UniProt: Q15116) fusion with a TEV site and a human Fc tag was cloned into pMax vector. The plasmids of mutated PD-1 were generated by a standard site-directed mutagenesis method (NEB, Ipswich, MA, USA) with a pair of primers for each mutation.

Protein expression and purification

Plasmids pMax-heavy_chain and pMax-light_chain of tislelizumab Fab were transiently cotransfected into HEK293F cells (Thermo Fisher) for protein expression. The supernatant was collected, and the tislelizumab Fab was purified by His tag affinity resin, followed by further purification with Superdex 200 (GE Healthcare, Shanghai, China) in a buffer containing 20 mM Tris and 150 mM NaCl (pH 8.0).

Plasmid pMax-PD-1 was transiently transfected into HEK293F cells (Thermo Fisher) for protein expression. The supernatant was collected, and the PD-1 was purified by protein A, followed by treatment with TEV Protease to remove the Fc tag. Then, the Fc-removed PD-1 was further purified with Superdex 200 (GE Healthcare) in a buffer containing 20 mM Tris and 150 mM NaCl (pH 8.0). The mutated PD-1 proteins were expressed and purified at similar condition as described above. The Fc tags of all PD-1 proteins used for SPR analysis were not removed.

Complex preparation and crystallization

The mammalian cell-expressed WT PD-1 protein and tislelizumab Fab fragment were mixed at a molar ratio of 1 : 1. The mixed sample was incubated for 30 min on ice and then purified by gel filtration in a buffer containing 20 mM Tris and 150 mM NaCl (pH 8.0). The complex peak was collected and concentrated to 30 mg·mL⁻¹, followed by crystal screening using the vapor-diffusion sitting-drop method at 20 °C. Diffracting crystals were obtained in a condition consisting of 0.1 M citric acid, pH 4.0, 1 M LiCl, and 20% PEG6000.

X-ray data collection and structural determination

The crystals were harvested with Nylon loops and immersed in the reservoir solution supplemented with 20% glycerol for 10 s and then were flash-cooled in liquid nitrogen. Diffraction data were collected at BL17U1, Shanghai Synchrotron Radiation Facility, and were processed with XDS program [21]. The phases were solved with program PHASER using structures of tislelizumab Fab fragment (our in-house structure not shown in this study) and PD-1 extracted from the complex structure of PD-1 with nivolumab Fab (PDB: 5WT9) [20] as the molecular replacement searching models. Phenix.refine was used to perform rigid body, TLS, and restrained refinement against X-ray data, followed by manual adjustment in COOT program and further refinement in Phenix.refine program [22,23]. The atomic coordinates and structural factors of PD-1/tislelizumab Fab complex have been deposited in the RCSB Protein Data Bank with accession number PDB: 7CGW.

SPR analysis

Surface plasmon resonance analysis was performed at room temperature using a BIAcore 8K system with CM5 chips (GE Healthcare). For all measurements, an HBS-EP plus buffer consisting of 10 mM HEPES, pH 7.4, 150 mM NaCl, 3 mM EDTA, and 0.005% (v/v) surfactant P20 was used as running buffer. The Fc-tagged PD-1 proteins were directly immobilized on the chip at a concentration of 150 nM. Gradient concentrations of antibody Fab (0, 1.56, 3.125, 6.25, 12.5, 25, 50, and 100 nM) were then flowed over the chip surface. After each cycle, the sensor surface was regenerated with 0.1 M glycine, pH 1.5. The binding kinetics were all analyzed with the software of BIA evaluation using a 1 : 1 steady-state affinity model.

P3Z assay

P3Z assay was carried out as previously described [24]. Briefly, HuT78/P3Z cells were preincubated with gradient concentrations of antibodies for 15 min prior to coculturing with HEK293/PD-L1 cells in 96-well plates (Costar, New York, NY, USA) containing complete RPMI 1640 media. The cells were incubated for 17 h at 37 °C. IL-2 secretion in the supernatants of coculture was assayed by ELISA using a kit from eBioscience according to the manufacturer's instructions.

Quantification and statistical analysis

Statistical analysis for the SPR and P3Z assays was analyzed with program Excel (Microsoft Corporation, Redmond, WA, USA) or program Prism (GraphPad Software, Inc, La Jolla, CA, USA).

Results

Tislelizumab shows remarkable antitumor efficacy in B16F10/GM-CSF mouse model

In this study, we evaluated the *in vivo* antitumor efficacy of tislelizumab in B16F10 melanoma-bearing mouse model. B16F10 melanoma cells overexpressing GM-CSF (B16F10/GM-CSF; 5×10^4) were implanted subcutaneously in hPD-1 C57BL/6 transgenic mice. PBS (vehicle) or tislelizumab (dose of 10 mg·kg⁻¹) was injected i.p. once a week, and tumor volumes were monitored twice a week. It was noted that five out of eight mice responded very well to tislelizumab treatment. The overall tumor growth of the tislelizumab-treated mice was significantly reduced in comparison with the vehicle group, resulting in approximate 86.7% tumor growth inhibition (TGI) with $P < 0.05$ (Fig. 1). This result revealed that tislelizumab exerted remarkable antitumor efficacy.

The dissociation rate of tislelizumab from PD-1 is much slower than that of pembrolizumab and nivolumab

In order to compare the binding affinity of tislelizumab, pembrolizumab, and nivolumab to PD-1, the binding kinetics of the three antibodies were investigated by SPR. As shown in Fig. 2 and Table 1, the association rate (K_a) of tislelizumab ($4.24 \times 10^5 \text{ M}^{-1} \cdot \text{s}^{-1}$) with PD-1 equals approximately twofold of that of nivolumab ($2.27 \times 10^5 \text{ M}^{-1} \cdot \text{s}^{-1}$) and one half of that of pembrolizumab ($9.54 \times 10^5 \text{ M}^{-1} \cdot \text{s}^{-1}$). However, the dissociation rate (K_d) of tislelizumab ($4.82 \times 10^{-5} \text{ s}^{-1}$) is about 30-fold slower than that of nivolumab ($1.57 \times 10^{-3} \text{ s}^{-1}$) and 80-fold less than of pembrolizumab ($3.88 \times 10^{-3} \text{ s}^{-1}$), respectively, resulting in a 35- to 60-fold higher target affinity of tislelizumab compared with the other two antibodies. At the same time, the $t_{1/2}$ of tislelizumab is 30- to 80-fold longer than that of pembrolizumab and nivolumab (Table 1). These results indicate that the high affinity of tislelizumab to PD-1 mainly results from its extremely slow dissociation rate from PD-1.

Unique epitopes of tislelizumab are identified by structural and SPR analyses

The remarkable antitumor activity of tislelizumab and its extremely slow dissociation property prompted our curiosity on the binding mechanism and epitopes of tislelizumab. To address this question, we cocrystallized the complex of tislelizumab Fab fragment with

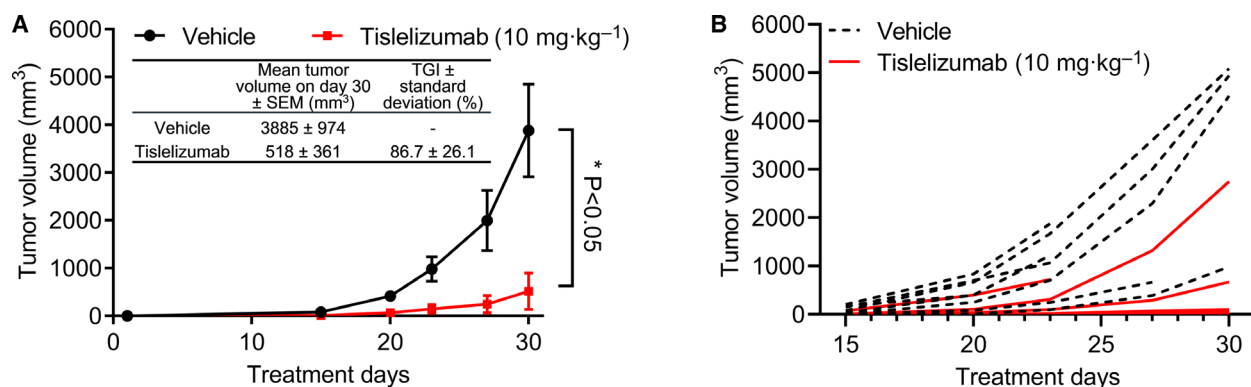


Fig. 1. Antitumor efficacy of tislelizumab in B16F10/GM-CSF hPD-1 transgenic mouse model. (A) Mice bearing B16F10/GM-CSF melanoma cells were treated i.p. with PBS (vehicle) or 10 mg·kg⁻¹ of tislelizumab once a week. Tumor volume was measured twice weekly. Data are presented as mean tumor volume ± standard error of the mean (SEM), $n = 8$ mice in each group. * $P < 0.05$ by two-tailed Student's t -test. (B) Tumor volume of individual mice is presented for the PBS (vehicle) and tislelizumab treatment group. Shortened lines indicate mice that were found dead or euthanized according to study protocol (Table S2).

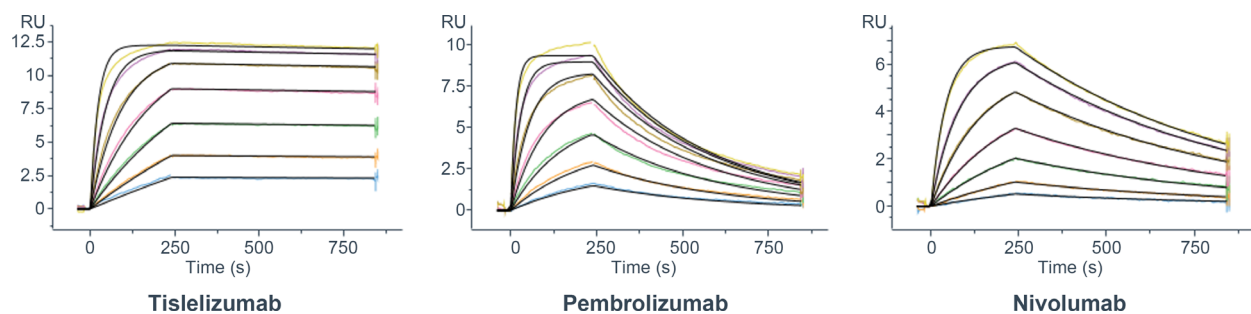


Fig. 2. SPR assay characterization of the binding affinity of tislelizumab, pembrolizumab, and nivolumab to PD-1. The data presented here are representatives of three independent experiments with similar results. RU, responsive unit.

Table 1. Binding kinetics of tislelizumab to WT PD-1 and its comparison with pembrolizumab and nivolumab. Data are presented as mean ± SEM of results of three independent experiments.

Sample	k_a (M ⁻¹ ·s ⁻¹)	k_d (s ⁻¹)	K_D (M)	$t_{1/2}$ (min)
Tislelizumab Fab	$4.24 \pm 0.094 \times 10^5$	$4.82 \pm 0.66 \times 10^{-5}$	$1.14 \pm 0.15 \times 10^{-10}$	248 ± 32
Pembrolizumab Fab	$9.54 \pm 1.2 \times 10^5$	$3.88 \pm 0.29 \times 10^{-3}$	$4.07 \pm 0.25 \times 10^{-9}$	3.0 ± 0.23
Nivolumab Fab	$2.27 \pm 0.063 \times 10^5$	$1.57 \pm 0.005 \times 10^{-3}$	$6.92 \pm 0.17 \times 10^{-9}$	7.3 ± 0.02

the ectodomain of PD-1, both of which were expressed in a mammalian cell system and solved the complex structure at a resolution of 3.2 Å (Table S1). The complex structure reveals that tislelizumab utilizes four of six complementarity-determining regions (CDRs) to interact with PD-1 (Fig. 3A) with a total buried surface of 2014 Å². All three CDR loops in the variable region of light chain (V_L) and CDR3 loop in the variable region of heavy chain (V_H) are involved in interaction with PD-1.

Based on this structural information, we carried out mutagenesis on a series of PD-1 residues observed to

potentially contribute to the PD-1/tislelizumab interaction, including Val64, Asn66, Met70, Ser71, Gln75, Thr76, Asp77, Lys78, Asp85, Arg86, Asp92, Ile126, Leu128, Lys131, and Ile134. The binding affinities of these mutated PD-1 proteins to tislelizumab were evaluated by SPR compared with WT PD-1. Meanwhile, pembrolizumab and nivolumab were also analyzed via SPR with the same PD-1 mutant proteins. The binding affinity of several mutated PD-1 proteins to tislelizumab significantly decreased compared with WT (Table 1 and Fig. 4A–I). Specifically, the K_D shift folds (K_D of mutation/ K_D of WT) of V64A, Q75A,

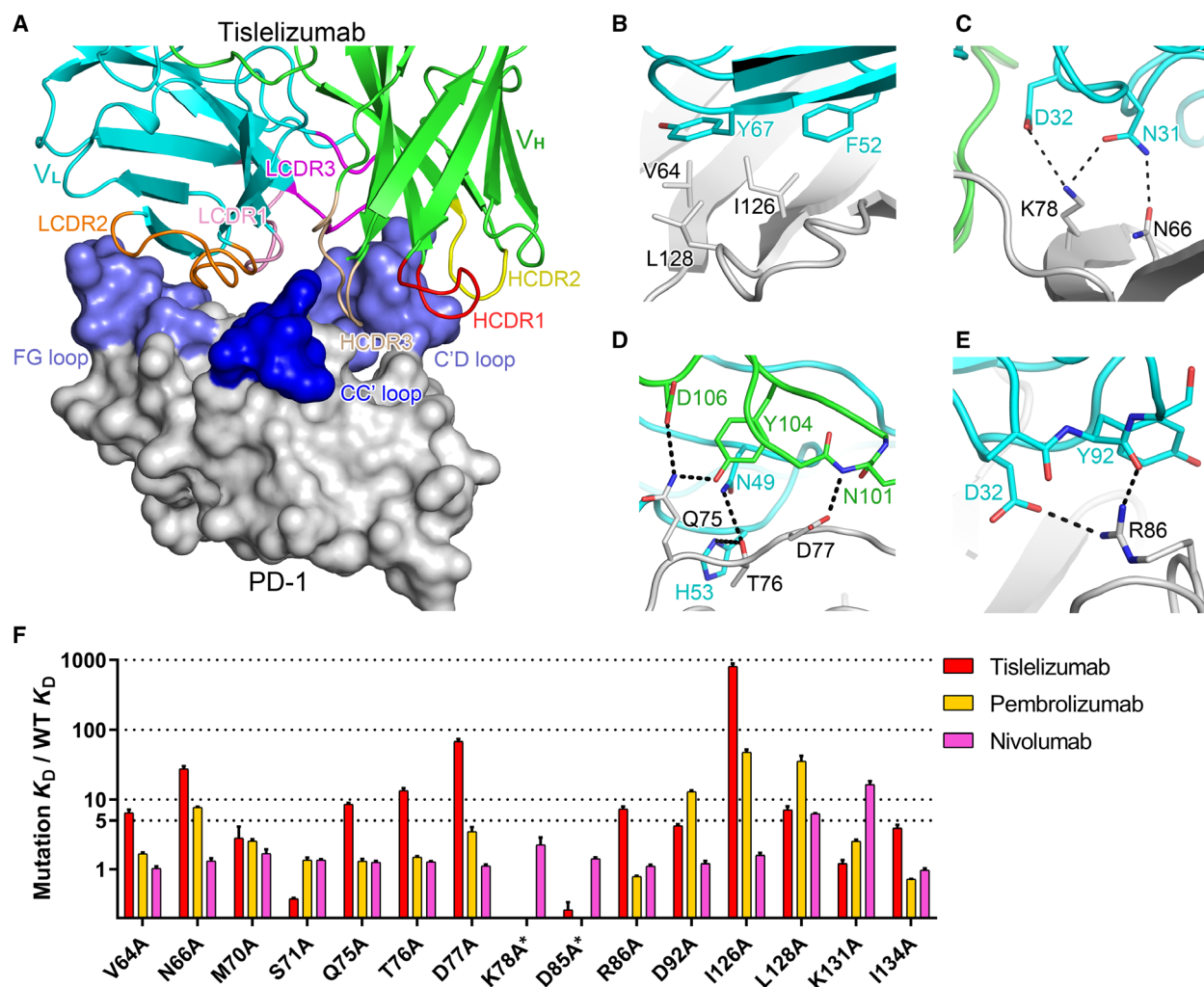


Fig. 3. Detailed interactions between tislelizumab and PD-1 and summary of SPR study. (A) The tislelizumab Fab is shown as ribbon (heavy chain, green; light chain, cyan), and PD-1 is shown as surface representation (gray). CC', C'D, and FG loops of PD-1 are highlighted in blue or light blue. The HCDR1, HCDR2, HCDR3, LCDR1, LCDR2, and LCDR3 of tislelizumab are colored in red, yellow, light golden, pink, orange, and magenta, respectively. (B–E) The PD-1, V_H, and V_L of tislelizumab are colored in gray, green, and cyan, respectively. Hydrogen bonds and a salt bridges are indicated as black dashed lines. (F) The SPR profile of tislelizumab, pembrolizumab, and nivolumab against PD-1 mutants. Data are presented as mean with SEM, $n = 3$. *, the K_D shift folds of tislelizumab and pembrolizumab against mutant K78A, as well as those of pembrolizumab against D85A, could not be accurately calculated due to no significant binding signal being detected during SPR analysis.

R86A, and L128A are more than 5, while the shift folds of N66A, T76A, and D77A range from 13 to 68, and that of I126A is nearly 800 (Fig. 3F and Table 2). The SPR results of other mutants with pembrolizumab and nivolumab are also summarized in Figs 3F and 4 and Table 2.

The detailed interactions between tislelizumab and residues V64, N66, Q75, T76, D77, R86, I126, and L128 of PD-1 are shown in Fig. 3B–E. The side chain of I126_{PD-1} forms a hydrophobic interaction with F52 in the tislelizumab light chain (F52_{LC}), and V64_{PD-1} and L128_{PD-1} interact with Y67_{LC} (Fig. 3B). In addition, a number of hydrogen bonds between N66_{PD-1}

and N31_{LC}, Q75_{PD-1} and Y104_{HC}, Q75_{PD-1} and D106_{HC}, T76_{PD-1} and N49_{LC}, T76_{PD-1} and H53_{LC}, D77_{PD-1} and N101_{HC}, and R86_{PD-1} and Y92_{LC}, and a salt bridge between R86_{PD-1} and D32_{LC} can further stabilize the PD-1/tislelizumab complex (Fig. 3C–E). Besides, K78_{PD-1} forms a hydrogen bond with N31_{LC} and a salt bridge with D32_{LC} (Fig. 3C). The K78A mutation in PD-1 abolishes the binding of PD-1 to tislelizumab (Fig. 4F). In conclusion, residues V64, N66, Q75, T76A, D77, K78, R86, I126, and L128 of PD-1 were identified as key epitopes of tislelizumab by structural biology and experimentally confirmed by SPR analysis. Notably, mutations Q75A, T76A,

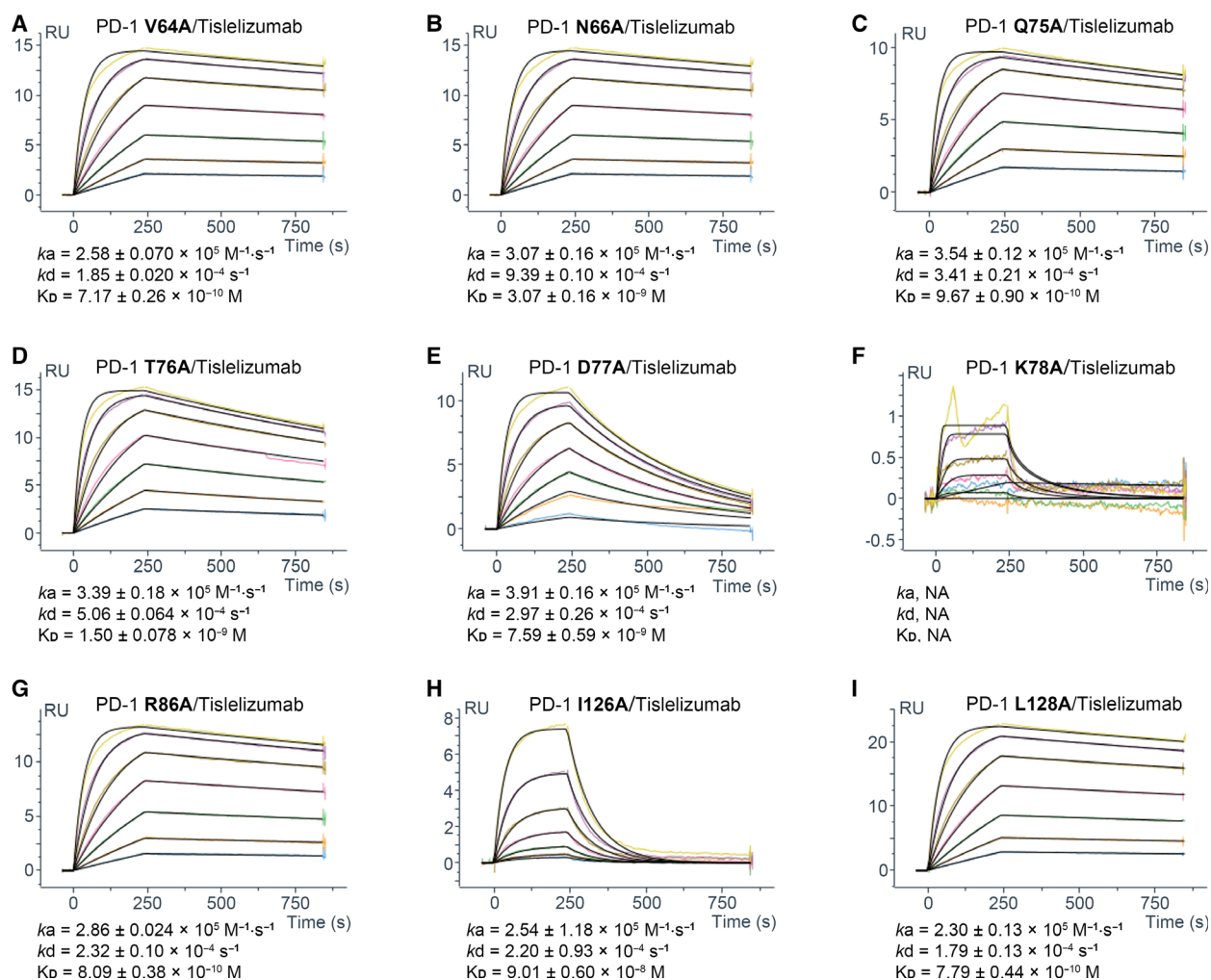


Fig. 4. The SPR profile of tislelizumab against specific PD-1 mutations in the epitope study. The data presented here are representatives of three independent experiments with similar results. The binding kinetics parameters are presented as the mean \pm SEM, $n = 3$. NA, the binding kinetics of tislelizumab against mutant K78A could not be accurately calculated due to no significant binding signal being detected during SPR analysis. RU, responsive unit.

D77A, and R86A only significantly affect the binding of tislelizumab rather than pembrolizumab and nivolumab (Fig. 3F and Table 2). Thus, residues Q75, T76, D77, and R86 of PD-1 were identified as unique binding epitopes for tislelizumab compared with pembrolizumab and nivolumab.

Tislelizumab is the first anti-PD-1 antibody targeting the CC' loop of PD-1

Notably, three of four unique epitopes, Q75, T76, and D77, are located at the CC' loop and adjacent area of PD-1 (Fig. 5). The C'D or FG loops have been reported to dominate binding by several antibodies [18,19,25–28]. However, the CC' loop, to our

knowledge, was never reported to bind with any anti-PD-1 antibody in previous publications.

The conformational change within the CC' loop is considered to be essential for PD-L1 binding to this loop [29,30]. Thus, it is reasonable that an antibody targeting this CC' loop could effectively abrogate PD-L1 binding to PD-1. However, no therapeutic anti-PD-1 antibodies were previously reported to bind to this loop. In the PD-1/tislelizumab complex, the CC' loop inserts into the space between HCDR3 and LCDR2, forming several hydrogen bonds between tislelizumab and PD-1 (Fig. 3A,D). Thus, this is the first time a therapeutic antibody is reported to interact with the CC' loop of PD-1, supplying a direct evidence that the CC' loop is an effective target region for therapeutic anti-PD-1 antibody.

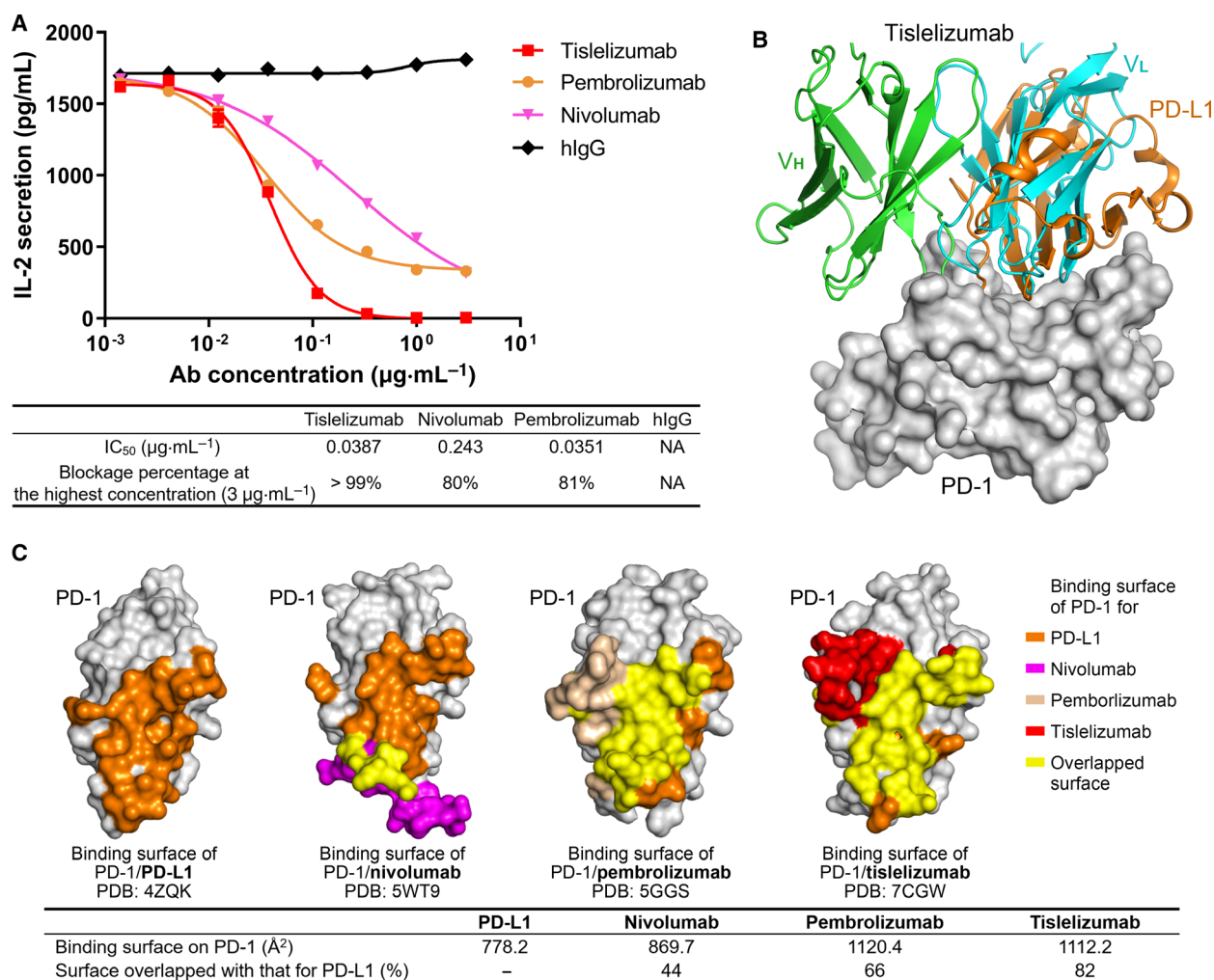


Fig. 6. Complete PD-L1 blockage of tislelizumab. (A) The PD-L1 blockage activity of tislelizumab in P3Z assay in comparison with pembrolizumab and nivolumab. HulgG was used as negative control. (B) Tislelizumab occupies the position of PD-L1 harboring PD-1. The heavy chain and light chain of V_H , tislelizumab Fab, PD-L1, and PD-1 are colored in green, cyan, orange, and gray, respectively. (C) Binding surface comparison between PD-L1, nivolumab, pembrolizumab, and tislelizumab. Surface of PD-1 molecule colored in orange, magenta, light golden, and red is the binding surface for PD-L1, nivolumab, pembrolizumab, and tislelizumab, respectively, while the surface colored in yellow marks the overlap area with the PD-L1/PD-1 interface.

(Fig. 3A). The detailed structural analysis and SPR results indicated that Q75A, T76A, and D77A mutations at the CC' loop and adjacent area of PD-1 significantly reduce the binding affinity to tislelizumab, but show much less effect on binding to pembrolizumab (Fig. 3F and Table 2), implying that the CC' loop of PD-1 plays a pivotal role in binding with tislelizumab, different from pembrolizumab. D85A, a mutation in the C'D loop of PD-1, completely disrupted PD-1 binding to pembrolizumab in the SPR experiment (Fig. S1I), which is consistent with a previous report [31]. However, D85A does not affect the binding affinity between PD-1 and tislelizumab (Fig. S1I and Table 2). By contrast, the R86A mutation at the same C'D loop showed no

impact on PD-1 binding to pembrolizumab, but caused sevenfold affinity decrease on that of tislelizumab (Table 2). SPR results of these two mutations indicate that, while both antibodies interact with the C'D loop of PD-1, they target different epitopes.

On the other hand, structural analysis showed that the binding surface of tislelizumab on PD-1 is quite different from that of nivolumab, with only a few overlapping residues. A comparative study between complex structures of PD-1 with tislelizumab and nivolumab also reveals that the two antibodies bind to PD-1 in two different orientations (Fig. 7). However, in our SPR results, those PD-1 mutations (V64A, N66A, Q75A, T76A, D77A, R86A, and I126A) that significantly

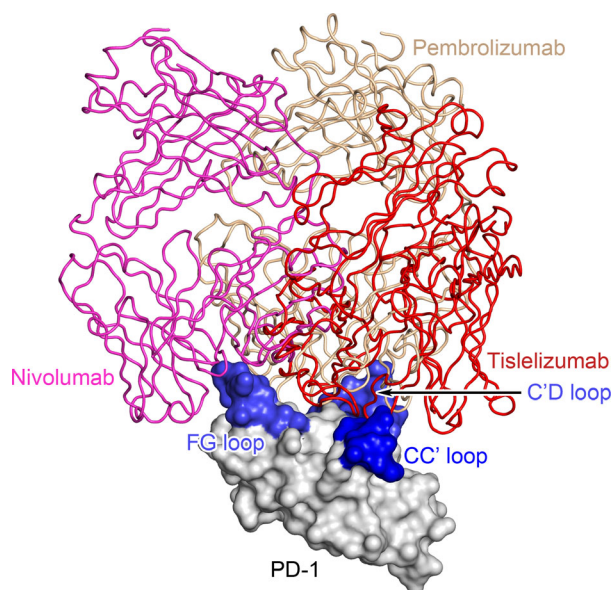


Fig. 7. Distinct binding orientation of tislelizumab compared with pembrolizumab and nivolumab. Superimposition of PD-1/tislelizumab complex with that of pembrolizumab (PDB: 5GGS) and nivolumab (PDB: 5WT9). PD-1, tislelizumab, pembrolizumab, and nivolumab are colored in gray, red, light golden, and magenta, respectively. The CC', C'D, and FG loops of PD-1 are highlighted in blue.

reduce the binding affinity to tislelizumab are not critical epitopes for nivolumab (Fig. 3F and Table 2).

Taken together, the structural analysis and SPR results demonstrate that tislelizumab has distinctive binding orientation to PD-1 and unique epitopes compared with pembrolizumab and nivolumab. From the SPR analysis summarized in Table 2, it is concluded that Gln75, Thr76, Asp77, and Arg86 of PD-1 are unique binding epitopes for tislelizumab compared with pembrolizumab and nivolumab. Notably, residues Gln75, Thr76, and Asp77 are all located at the CC' loop and its adjacent area of PD-1.

It has been previously reported that pembrolizumab binds to the C'D loop of PD-1, while nivolumab mainly binds to the N loop [18–20,25]. Recently, Liu *et al.* [27] reported that toripalimab, an antibody generated by Shanghai Junshi Bioscience, binds to the FG loop of PD-1. Besides, several preclinical stage anti-PD-1 antibodies were reported to bind with the BC, C'D, or FG loops [26,28,32]. All the four loops referred above are far away from the CC' loop in PD-1 (Fig. 5). In contrast to all of the reported anti-PD-1 antibodies, tislelizumab is the first antibody that interacts with the CC' loop of PD-1.

The CC' loop of PD-1 is considered to play a critical role in the binding of PD-1 to PD-L1, and it undergoes a significant conformational change and

transforms from an open conformation to a closed one after binding with PD-L1 [29]. It has been reported that this conformational change in the CC' loop could stabilize the interaction of PD-1 with PD-L1 and influence their binding affinity [29,30]. As the mutations at the CC' loop of PD-1 significantly accelerated the off-rate of tislelizumab and reduced its binding affinity in SPR (Fig. 4 and Table 1), we also speculate that the direct binding to the CC' loop might contribute to the high affinity and slow off-rate of tislelizumab. Taken together, the unique epitopes on the CC' loop of PD-1 contribute to the observation that tislelizumab completely blocks PD-1/PD-L1 interaction, while both nivolumab and pembrolizumab only show partial PD-L1 blocking activity in the cellular assay (Fig. 6A).

Conclusion

In summary, we report the remarkable antitumor efficacy of tislelizumab in tumor model and key epitopes of tislelizumab identified by both structural biology and SPR analysis. Distinct from all currently approved anti-PD-1 antibodies, tislelizumab uniquely binds to the CC' loop of PD-1, which is the first time to be reported to interact with an anti-PD-1 antibody. In addition, tislelizumab displays complete blocking activity to PD-L1 with extremely slow dissociation rate from PD-1, and its binding surface largely overlaps with that of PD-L1. All these findings facilitate our understanding of the binding mechanisms of tislelizumab and provide a novel targetable region for the development of anti-PD-1 antibodies for tumor immunotherapy.

Acknowledgements

We gratefully acknowledge the X-ray Crystallography Platform at the Institute of Biophysics and beamline staff members at BL17U1 of SSRF for technical support with diffraction data collection. This research received no external funding.

Conflict of interest

The authors declare no conflict of interest.

Data accessibility

The atomic coordinates and structural factors of PD-1/tislelizumab Fab complex have been deposited at the RCSB Protein Data Bank with accession number PDB: 7CGW.

Author contributions

TZ, KL, ML, and YL conceived and designed this project. YH and YF performed X-ray crystallography. HS analyzed the structure. BZ carried out SPR assays. HW expressed and purified PD-1 mutant proteins. TZ, YL, and QZ designed and performed the P3Z assay. YZ, XC, ZL, and XS conducted the *in vivo* efficacy study. YH, HS, and YL wrote the manuscript. YL supervised this study.

References

- Greenwald RJ, Freeman GJ and Sharpe AH (2005) The B7 family revisited. *Annu Rev Immunol* **23**, 515–548.
- Zou W and Chen L (2008) Inhibitory B7-family molecules in the tumour microenvironment. *Nat Rev Immunol* **8**, 467–477.
- Chen L and Flies DB (2013) Molecular mechanisms of T cell co-stimulation and co-inhibition. *Nat Rev Immunol* **13**, 227–242.
- Iwai Y, Ishida M, Tanaka Y, Okazaki T, Honjo T and Minato N (2002) Involvement of PD-L1 on tumor cells in the escape from host immune system and tumor immunotherapy by PD-L1 blockade. *Proc Natl Acad Sci USA* **99**, 12293–12297.
- Blackburn SD, Shin H, Haining WN, Zou T, Workman CJ, Polley A, Betts MR, Freeman GJ, Vignali DA and Wherry EJ (2009) Coregulation of CD8⁺ T cell exhaustion by multiple inhibitory receptors during chronic viral infection. *Nat Immunol* **10**, 29–37.
- Schildberg FA, Klein SR, Freeman GJ and Sharpe AH (2016) Coinhibitory pathways in the B7-CD28 ligand-receptor family. *Immunity* **44**, 955–972.
- Pardoll DM (2012) The blockade of immune checkpoints in cancer immunotherapy. *Nat Rev Cancer* **12**, 252–264.
- Freeman GJ, Long AJ, Iwai Y, Bourque K, Chernova T, Nishimura H, Fitz LJ, Malenkovich N, Okazaki T, Byrne MC *et al.* (2000) Engagement of the PD-1 immunoinhibitory receptor by a novel B7 family member leads to negative regulation of lymphocyte activation. *J Exp Med* **192**, 1027–1034.
- Latchman YWC (2001) PD-L2 is a second ligand for PD-1 and inhibits T cell activation. *Nat Immunol* **2**, 261–268.
- Powles T, Eder JP, Fine GD, Braithel FS, Loriot Y, Cruz C, Bellmunt J, Burris HA, Petrylak DP, Teng SL *et al.* (2014) MPDL3280A (anti-PD-L1) treatment leads to clinical activity in metastatic bladder cancer. *Nature* **515**, 558–562.
- Chen L and Han X (2015) Anti-PD-1/PD-L1 therapy of human cancer: past, present, and future. *J Clin Invest* **125**, 3384–3391.
- Garon EB (2015) Pembrolizumab for the treatment of non-small-cell lung cancer. *N Engl J Med* **372**, 2018–2028.
- Gunturi A and McDermott DF (2015) Nivolumab for the treatment of cancer. *Expert Opin Investig Drugs* **24**, 253–260.
- Li Y, Li F, Jiang F, Lv X, Zhang R, Lu A and Zhang G (2016) A mini-review for cancer immunotherapy: molecular understanding of PD-1/PD-L1 pathway & translational blockade of immune checkpoints. *Int J Mol Sci* **17**, 1151–1172.
- Zou W, Wolchok JD and Chen L (2016) PD-L1 (B7-H1) and PD-1 pathway blockade for cancer therapy: mechanisms, response biomarkers, and combinations. *Sci Transl Med* **8**, 328rv4.
- Callahan MK, Postow MA and Wolchok JD (2016) Targeting T cell co-receptors for cancer therapy. *Immunity* **44**, 1069–1078.
- Lee A and Keam SJ (2020) Tislelizumab: first approval. *Drugs* **80**, 617–624.
- Lee JY, Lee HT, Shin W, Chae J, Choi J, Kim SH, Lim H, Won Heo T, Park KY, Lee YJ *et al.* (2016) Structural basis of checkpoint blockade by monoclonal antibodies in cancer immunotherapy. *Nat Commun* **7**, 13354.
- Na Z, Yeo SP, Bharath SR, Bowler MW, Balicci E, Wang CI and Song H (2017) Structural basis for blocking PD-1-mediated immune suppression by therapeutic antibody pembrolizumab. *Cell Res* **27**, 147–150.
- Tan S, Zhang H, Chai Y, Song H, Tong Z, Wang Q, Qi J, Wong G, Zhu X, Liu WJ *et al.* (2017) An unexpected N-terminal loop in PD-1 dominates binding by nivolumab. *Nat Commun* **8**, 14369.
- Kabsch W (2010) Xds. *Acta Crystallogr D Biol Crystallogr* **66**, 125–132.
- Emsley P, Lohkamp B, Scott WG and Cowtan K (2010) Features and development of Coot. *Acta Crystallographica Section D* **66**, 486–501.
- Afonine PV, Grosse-Kunstleve RW, Echols N, Headd JJ, Moriarty NW, Mustyakimov M, Terwilliger TC, Urzhumtsev A, Zwart PH and Adams PD (2012) Towards automated crystallographic structure refinement with phenix.refine. *Acta Crystallogr D Biol Crystallogr* **68**, 352–367.
- Zhang T, Song X, Xu L, Ma J, Zhang Y, Gong W, Zhang Y, Zhou X, Wang Z, Wang Y *et al.* (2018) The binding of an anti-PD-1 antibody to FcγRI has a profound impact on its biological functions. *Cancer Immunol Immunother* **67**, 1079–1090.
- Horita S, Nomura Y, Sato Y, Shimamura T, Iwata S and Nomura N (2016) High-resolution crystal structure of the therapeutic antibody pembrolizumab bound to the human PD-1. *Sci Rep* **6**, 35297.

- 26 Chen D, Tan S, Zhang H, Wang H, He W, Shi R, Tong Z, Zhu J, Cheng H, Gao S *et al.* (2019) The FG Loop of PD-1 serves as a "hotspot" for therapeutic monoclonal antibodies in tumor immune checkpoint therapy. *iScience* **14**, 113–124.
- 27 Liu H, Guo L, Zhang J, Zhou Y, Zhou J, Yao J, Wu H, Yao S, Chen B, Chai Y *et al.* (2019) Glycosylation-independent binding of monoclonal antibody toripalimab to FG loop of PD-1 for tumor immune checkpoint therapy. *MAbs* **11**, 681–690.
- 28 Liu J, Wang G, Liu L, Wu R, Wu Y, Fang C, Zhou X, Jiao J, Gu Y, Zhou H *et al.* (2019) Study of the interactions of a novel monoclonal antibody, mAb059c, with the hPD-1 receptor. *Sci Rep* **9**, 17830.
- 29 Zak KM, Kitel R, Przetocka S, Golik P, Guzik K, Musielak B, Domling A, Dubin G and Holak TA (2015) Structure of the complex of human programmed death 1, PD-1, and its ligand PD-L1. *Structure* **23**, 2341–2348.
- 30 Kundapura SV and Ramagopal UA (2019) The CC' loop of IgV domains of the immune checkpoint receptors, plays a key role in receptor:ligand affinity modulation. *Sci Rep* **9**, 19191.
- 31 Na Z, Yeo SP, Bharath SR, Bowler MW, Balıkcı E, Wang C-I and Song H (2017) Structural basis for blocking PD-1-mediated immune suppression by therapeutic antibody pembrolizumab. *Cell Res* **27**, 147–150.
- 32 Wang M, Wang J, Wang R, Jiao S, Wang S, Zhang J and Zhang M (2019) Identification of a monoclonal antibody that targets PD-1 in a manner requiring PD-1 Asn58 glycosylation. *Commun Biol* **2**, 392.

Supporting information

Additional supporting information may be found online in the Supporting Information section at the end of the article.

Fig. S1. The SPR profile of tislelizumab, pembrolizumab and nivolumab against PD-1 mutants. The data presented here are representatives of three independent experiments with similar results. RU, responsive units.

Table S1. Data collection and refinement statistics.

Table S2. The original tumor measurement data of the *in vivo* efficacy study.